Interaction-Driven Spectrum Reconstruction in Bilayer Graphene

A. S. Mayorov, *et al.*

Science **333**, 860 (2011);
DOI: 10.1126/science.1208683

Interaction-Driven Spectrum Reconstruction in Bilayer Graphene

A. S. Mayorov,[1] D. C. Elias,[1] M. Mucha-Kruczynski,[2] R. V. Gorbachev,[3] T. Tudorovskiy,[4] A. Zhukov,[3] S. V. Morozov,[5] M. I. Katsnelson,[4] V. I. Fal'ko,[2] A. K. Geim,[3] K. S. Novoselov[1]*

The nematic phase transition in electronic liquids, driven by Coulomb interactions, represents a new class of strongly correlated electronic ground states. We studied suspended samples of bilayer graphene, annealed so that it achieves very high quasiparticle mobilities (greater than 10^6 square centimers per volt-second). Bilayer graphene is a truly two-dimensional material with complex chiral electronic spectra, and the high quality of our samples allowed us to observe strong spectrum reconstructions and electron topological transitions that can be attributed to a nematic phase transition and a decrease in rotational symmetry. These results are especially surprising because no interaction effects have been observed so far in bilayer graphene in the absence of an applied magnetic field.

Although many consequences of the chiral nature of the quasiparticles in mono- (*1*–*3*) and bilayer (*4*–*5*) graphene have already been demonstrated (*3*), sample inhomogeneities and broadening of the energy levels (due to a finite lifetime of the charge carriers) prohibited direct access to the intriguing regime of zero electron and hole concentrations. The latter regime has attracted a large number of possible scenarios for the particular arrangement of the electron ground state. For bilayer graphene, the single-electron picture (*5*) (where the parabolic spectrum is replaced by four Dirac cones at low energies) is challenged by several many-body phase transition scenarios: ferromagnetic (*6*), ferroelectric (*7*, *8*), and nematic (*9*, *10*). The latter resembles the transitions in correlated anisotropic electron fluids (*11*–*13*) that have been observed in several systems, including electrons in high Landau levels in two-dimensional electron gas (*14*–*16*), multilayered complex oxides (*17*, *18*), iron pnictides (*19*), and strontium ruthenate (*20*).

Recently, the required access to the low-energy physics in bilayer crystals has been enabled by improvements in the quality of samples created by removing the underlying substrate (*21*–*23*). Free-standing graphene devices allow a 100-fold increase in the mobility (above 10^6 cm^2/V·s) (*24*) after annealing. We studied the low-energy electronic properties of such high-quality, free-standing bilayer graphene devices and demonstrate that electron-electron interaction effects play a dominant role at low energies, even at low magnetic fields strengths B. Our samples were prepared on Si/SiO_2 substrate (300 nm of SiO_2) by micromechanical cleavage (*1*). Narrow (2 to 4 μm) ribbons were selected, and Cr/Au (5 nm/150 nm) contacts were deposited by means of electron-beam or laser-writer lithography and electron-beam evaporation to create two-probe devices. Wet etching in buffered hydrofluoric acid was used to remove about 150 nm of SiO_2 substrate to form free-standing bilayer graphene devices (Fig. 1C).

As prepared, such samples were p-doped to about several 10^{12} cm^{-2} and exhibited mobility traditionally expected for samples on a substrate (*25*) (~5000 cm^2/V·s). We used current annealing (*22*) to remove such unintentional doping and increase the mobility (typically 0.5 to 1 mA/μm current densities were used). After annealing, our devices exhibited a very sharp resistance peak situated almost exactly at zero gate voltage (within 10^8 cm^{-2} in terms of residual doping; Fig. 1, A and B). Typical quantum mobilities achieved were within $\mu_q = 0.5 \times 10^6$ to 1.5×10^6 cm^2/V·s (estimated from the onset of quantum oscillations in magnetic field B_0 as $\mu_q B_0 = 1$). Transport mobilities were more difficult to estimate because of the influence of the contacts in the two-probe geometry and nearly ballistic transport in our high-quality samples. However, a rough estimate made from the slope of the conductivity curve (field effect mobility: $\mu = 1/e \cdot d\sigma/dn$, where σ is conductivity) gave similar numbers (within 30%).

Our experiments on electronic transport in free-standing bilayer graphene in zero and finite magnetic fields show that at energies below 5 meV, the parabolic dispersion [as usually observed at high energies (*4*)] is replaced, through an electron topological transition, by several pockets with a linear spectrum. Also, our magnetic field measurements show the presence of only two Dirac cones around each K point in the Brillouin zone, in contrast with the single-particle theory (*5*) that predicts four Dirac cones around each K point at energies below 1 meV. We interpret the results of our experiments as an indication for interaction-driven phase transition (*9*).

All of the samples in our study had practically zero doping (within 10^8 cm^{-2}), which allowed us to estimate the possible energy gap that would arise from asymmetry between the layers. This gap is lower than 0.1 meV, which is an order of magnitude smaller than the effects we describe. The absence of the gap is also manifested in the relatively weak temperature dependence of the resistivity peak (conductivity minimum) down to the lowest temperatures measured (T = 0.25 K) (Figs. 1A and 2A). At low temperatures, the conductivity saturates at a finite value of about 20 $e^2/\pi h$ (h, Planck's constant) (see fig. S1 for details), which is substantially greater than the value expected for ballistic monolayer graphene (*26*, *27*) ($4e^2/\pi h$) or bilayer graphene with a parabolic dispersion relation (*28*) ($8e^2/\pi h$). The measured minimum conductivity is slightly lower than $24e^2/\pi h$ predicted (*29*) for bilayer spectrum transformed by the electron topological transition at low Fermi energies (*5*) (Fig. 2B).

The broadening and the amplitude of the conductivity minimum were linear functions of temperature for $T > 20$ K. Broadening of the conductivity minimum effectively yielded the same information as the amplitude, but without the ambiguity that arises from the contact resistance and the quantum minimum conductivity (see SOM text for the definition of broadening we use here). Such behavior is expected for the parabolic dispersion relation, which guarantees a constant density of states (conductivity: $\sigma_{min} = e\mu\int D(E)[f(E,T) - f(E,T=0)]dE = 4\ln(2)e\mu mT/\pi\hbar^2$, where $D(E)$ = constant is the density of states, $f(E,T)$ is the Fermi-Dirac distribution function, and m is the effective mass, and we assumed that the mobility is independent of the temperature and the position of the

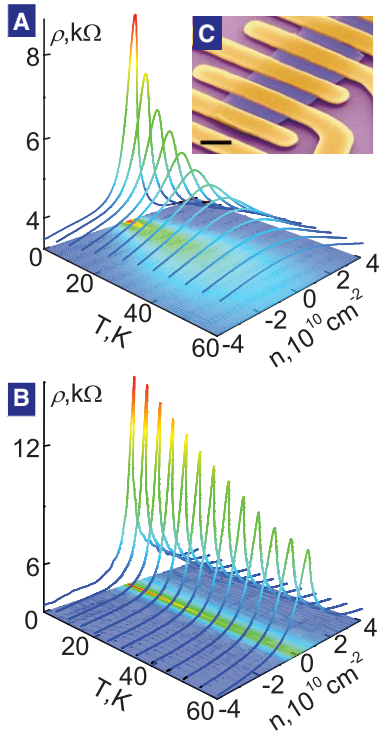

Fig. 1. Temperature dependence of the resistance in graphene and bilayer graphene. (**A**) Temperature dependence of two-terminal resistance of bilayer graphene at zero magnetic field. (**B**) Temperature dependence of two-probe resistance of monolayer graphene at zero magnetic field. (**C**) A scanning electron micrograph of one of our suspended devices.

[1]School of Physics and Astronomy, University of Manchester, Manchester M13 9PL, UK. [2]Physics Department, Lancaster University, Lancaster LA1 4YB, UK. [3]Manchester Centre for Mesoscience and Nanotechnology, University of Manchester, Manchester M13 9PL, UK. [4]Radboud University of Nijmegen, Institute for Molecules and Materials, Heyendaalseweg 135, 6525 AJ Nijmegen, Netherlands. [5]Institute for Microelectronics Technology, 142432 Chernogolovka, Russia.

*To whom correspondence should be addressed. E-mail: kostya@manchester.ac.uk

Fermi level). The slope of the temperature dependence yielded $m \approx (0.029 \pm 0.003)m_0$ (Fig. 2B) (here m_0 is the free electron mass). Note that according to the same arguments, the conductivity for the monolayer graphene and broadening of the conductivity minimum increased much more slowly and [because $D(E) \propto |E|$ for the linear spectrum] is a parabolic function of T (Fig. 1B and Fig. 2, B and C).

For $T < 20$ K, the temperature dependence of the width of the conductivity minimum for bilayer graphene was substantially weaker than what is expected for the parabolic dispersion relation (the amplitude of the conductivity minimum yields a similar conclusion). A slow T dependence hints that the density of states at low energy is suppressed, although it remains finite. Such behavior has been predicted (*5*) for the low-energy part of the bilayer spectrum, below the saddle-point E^* in the electron dispersion, where the high-energy parabolic spectrum is replaced by four Dirac minicones (see inset to Fig. 2B); the value of E^* is determined by the amplitude of the next-nearest neighbor interlayer hopping γ_3, and the number of pockets by the trigonal symmetry of this parameter.

A change in the band structure topology, which consists of a single-connected isoenergetic line splitting into disconnected parts, is known as the electron topological or Lifshitz transition (*30*). In bilayer graphene, such a transition is expected to occur at $E^* \sim 1$ meV, yielding the temperature dependence presented in Fig. 2A (green curve). Although such theoretical prediction qualitatively captures the general trend (transition from parabolic to linear temperature dependence), it strongly underestimates the value of E^*. It requires E^* on the order of 6 meV to fit our experimental data (Fig. 2A, red curve; see below for the details of the model used).

To study the electron topological transition in more detail and search for evidence of many-body effects, we measured the transport properties of such high-quality bilayer samples in an applied magnetic field. Our measurements are summarized in Fig. 3, where the resistivity is plotted as a function of magnetic field and gate voltage. We observed nonmonotonic changes in resistivity at filling factor $\nu = 0$ (Fig. 3B). The sign of magnetoresistance changed twice: It was positive at low (<0.1 T) and high (>0.3 T) magnetic fields and negative in the intermediate region. Generally, higher-quality samples exhibited these features at lower fields. We interpret the divergence of the resistance at high fields ($B >$ 0.3 T) as the gap opening at $\nu = 0$, similar to that observed previously (*23, 31*). The negative magnetoresistance at $0.1 \text{ T} < B < 0.3$ T has a resonant character—a narrow cusp appears in resistance in a narrow area of concentrations ($\pm 2 \times 10^9$ cm^{-2}) (Fig. 3C and figs. S2 and S3), an effect that we cannot explain at present. Data for a device with different mobility is shown in fig. S2.

We also observed that the cyclotron gaps at filling factor $\nu = \pm 4$ (the filling factor is determined from the carrier concentration n as $\nu = nh/eB$) were much more robust than the gaps at other filling factors and could be observed at magnetic fields as low as 100 G [the other filling factors are observed only at $B > 0.4$ T even for the highest-quality samples, which is consistent with the results obtained by other groups (*31*)]. Figure 4 summarizes our measurements of the cyclotron gaps at various filling factors (obtained from fitting of the temperature dependence of oscillations presented in Fig. 3C with the Lifshitz-Kosevich formula). The cyclotron gaps at filling factors ±8, ±12, ±16, ±20, and ±24 showed a linear dependence on magnetic field (Fig. 4). We extracted the corresponding cyclotron mass, which appears to be $m = (0.028 \pm 0.002)m_0$—close to the previously reported value for nonsuspended samples (*32*). At the same time, the gap for $\nu = \pm 4$ rose quickly for $0 \text{ T} < B < 0.02$ T and then stayed practically constant at $E_L \approx 5.5$ meV for $0.02 \text{ T} < B < 0.8$ T, before increasing linearly with a slope ~40% greater than that for other filling factors.

The reported observation cannot be explained within the framework of parabolic bands, which predicts roughly equidistant Landau levels. It also contradicts the more elaborative theory (*5*) (beyond the nearest-neighbor hopping approximation), which predicts four Dirac minicones below the electron topological transition energy in the vicinity of both K and K′ points. Similar to graphene, each of such Dirac pockets would result in a doubly degenerate Landau level, so the total degeneracy of the zero Landau level is 16, and the largest cyclotron gap should correspond to filling factor ±8, instead of ±4 as observed in our experiments.

To explain the observed eight-fold degeneracy of the lowest Landau level, we need to assume that the rotational symmetry of the system is lowered by, e.g., the nematic phase transition (*9*, *10*), which results in the following Hamiltonian for the low-energy electrons,

$$H = -\frac{1}{2m}\begin{pmatrix} 0 & (\pi^\dagger)^2 \\ \pi^2 & 0 \end{pmatrix} + \xi v_3 \begin{pmatrix} 0 & \pi \\ \pi^\dagger & 0 \end{pmatrix} + \begin{pmatrix} 0 & u \\ u & 0 \end{pmatrix}$$

and reduces the number of low-energy Dirac minicones from four to two near each of the

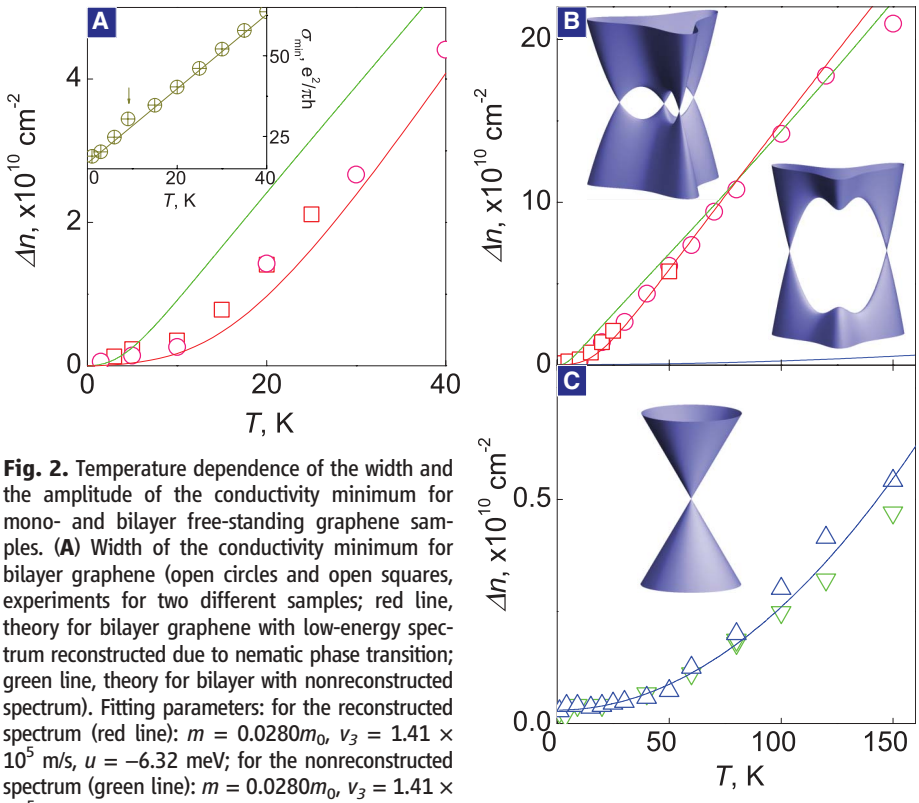

Fig. 2. Temperature dependence of the width and the amplitude of the conductivity minimum for mono- and bilayer free-standing graphene samples. (**A**) Width of the conductivity minimum for bilayer graphene (open circles and open squares, experiments for two different samples; red line, theory for bilayer graphene with low-energy spectrum reconstructed due to nematic phase transition; green line, theory for bilayer with nonreconstructed spectrum). Fitting parameters: for the reconstructed spectrum (red line): $m = 0.0280m_0$, $v_3 = 1.41 \times 10^5$ m/s, $u = -6.32$ meV; for the nonreconstructed spectrum (green line): $m = 0.0280m_0$, $v_3 = 1.41 \times 10^5$ m/s, $u = 0$. (Inset) Amplitude of the conductivity minimum of bilayer graphene (yellow crossed circles, experiment; yellow solid line, a guide to the eye). Note the deviation from the straight line below 10 K (marked by arrow). (**B**) The broadening of the conductivity minimum for bilayer samples [circles, squares, and red and green lines are the same as in (A) and for monolayer graphene (blue line, theory)]. (Insets) Left: Low-energy electronic spectrum as expected in the single-electron approximation; right: bilayer graphene low-energy electronic spectrum, reconstructed due to nematic phase transition. (**C**) The broadening of the conductivity minimum for monolayer graphene [blue and green triangles: experimental points for two different samples; blue line: theory, same as in (B)]. (Inset) Low-energy electronic spectrum for monolayer graphene.

two K points (Fig. 4A). In the above Hamiltonian, ξ differentiates between the two valleys, v_3 is the velocity associated with the interlayer skew hopping (*5*), and u is the order parameter formed upon nematic phase transition. This transition is driven by Coulomb interaction between electrons (the strength of which is partly reduced by screening), and it has been established by the renormalization-group study of bilayer parameters and the strength of the interaction between all types of symmetry-breaking fluctuation in the electronic liquid in bilayer graphene (*9*, *10*). We could fit our experimental results for the cyclotron gaps rather accurately (Fig. 4, B and C). The range of parameters that fit our results was very narrow, and the same set of parameters fit our temperature broadening data at zero magnetic field (Fig. 2, A and B).

Lowering of the symmetry can be expected, either in the case of the spontaneous symmetry breaking caused by many-body effects or in the case of mechanical deformation of our devices, either by uniaxial strain of the whole crystal (*33*) or by interlayer shear shift (*34*) caused by their preparation or handling history. However, the latter scenario can be ruled out because the strain required to explain the results observed in our work could be estimated (*33*) to be on the order of 1%, whereas the typical strain found in similar devices (prepared and handled in the same

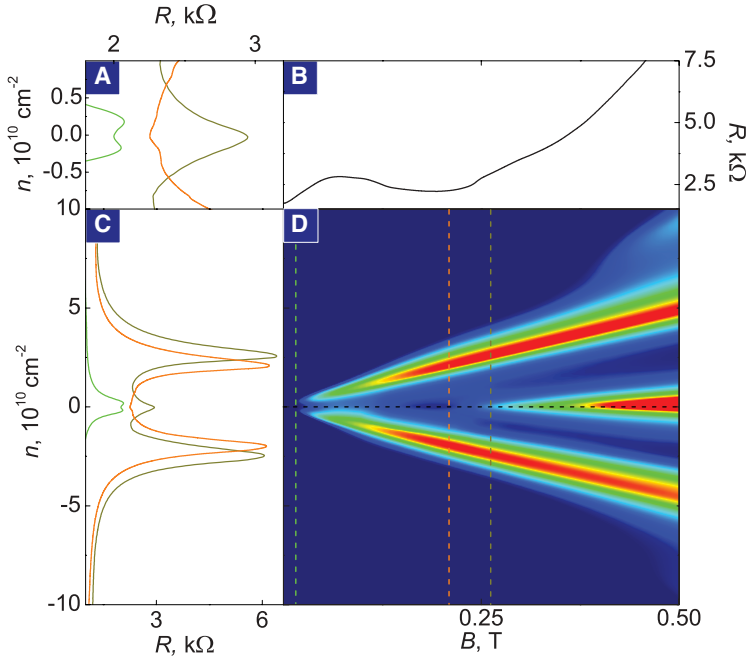

Fig. 3. Free-standing bilayer samples in magnetic field. (**A**) Resistance of suspended bilayer graphene as a function of gate voltage (recalculated to carrier concentration) for B = 0.01 T (green), B = 0.2 T (orange), and B = 0.26 T (dark yellow). (**B**) Resistance of suspended bilayer graphene at ν =0 as a function of magnetic field. (**C**) Same as (A) for a greater span of the carrier concentration. (**D**) Contour map of resistance of free-standing bilayer graphene device as a function of carrier concentration and magnetic field. The resistance spans from 2.1 kilohm (blue) to 6 kilohm (red). The three vertical lines correspond to the positions of the B = 0.01 T (green), B = 0.2 T (orange), and B = 0.26 T (dark yellow) in (A) and (C).

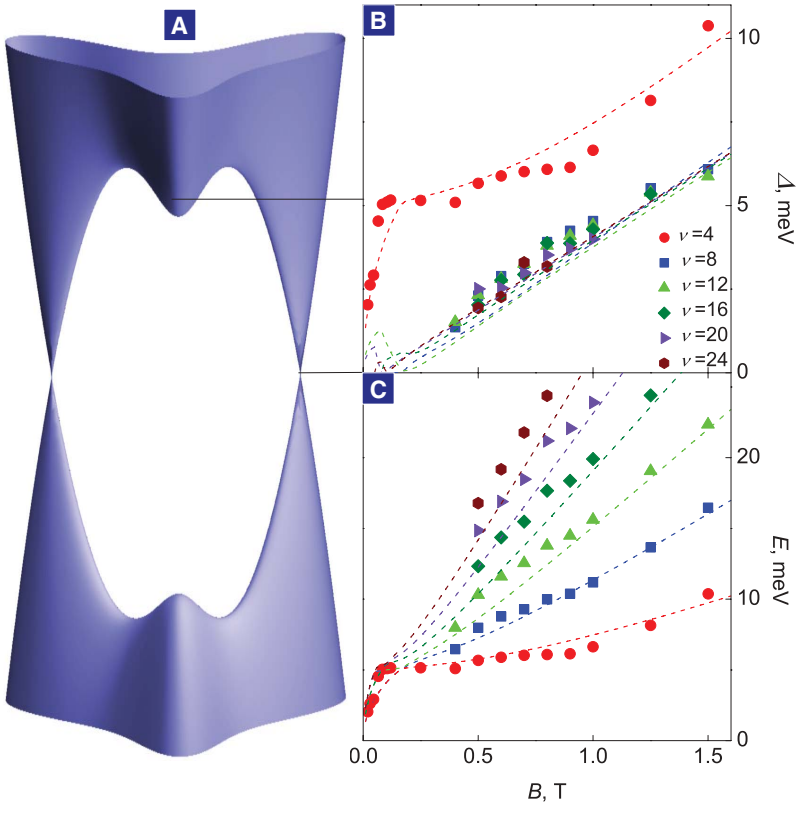

Fig. 4. (**A**) Low-energy electron spectrum for graphene bilayer, reconstructed due to nematic phase transition. (**B**) Cyclotron gaps for different filling factors. Symbols (experiment) and curves (theory) of the same color correspond to the same filling factor (fitting parameters: $m = 0.0280m_0$, $v_3 = 1.41 \times 10^5$ m/s, u = −6.32 meV). (**C**) The position of the Landau levels as a function of magnetic field, recalculated from (B). Symbols (experiment) and curves (theory) of the same color correspond to the same filling factor as in (B).

way) was measured (*24*) and was <0.1%. Moreover, in the case of externally induced strain, the direction of mechanical deformations would be related to the contact geometry, not to the crystallographic orientation, and would vary from sample to sample. Instead, we find the same feature in four different devices, which would require a rather narrow range of parameters (size and orientation of the principal axes of strain tensor) to be repeated precisely in different samples. We also have considered whether our results can be explained in terms of a spontaneous gap opening in the bilayer spectrum (*35*). In this case, the transport at the neutrality point (with or without magnetic field) would be dominated by a network of one-dimensional channels between the domains of gaps with alternating signs. This would result in a minimum conductivity value that depends strongly on the strain prehistory, in contrast to values reproducibly observed in our experiments. Also, this model would not likely produce a drop in the resistance at $\nu = 0$, as observed in our experiments. These differences suggest that the observed reconstruction of the spectrum is the result of an intrinsic modification of the electronic system; in particular, it can be caused by the recently predicted "nematic" phase transition (*9*, *10*) in bilayer graphene.

References and Notes

1. K. S. Novoselov *et al.*, *Science* **306**, 666 (2004).
2. A. K. Geim, K. S. Novoselov, *Nat. Mater.* **6**, 183 (2007).
3. A. H. Castro Neto, F. Guinea, N. M. R. Peres, K. S. Novoselov, A. K. Geim, *Rev. Mod. Phys.* **81**, 109 (2009).
4. K. S. Novoselov *et al.*, *Nat. Phys.* **2**, 177 (2006).
5. E. McCann, V. I. Fal'ko, *Phys. Rev. Lett.* **96**, 086805 (2006).
6. E. V. Castro, N. M. R. Peres, T. Stauber, N. A. P. Silva, *Phys. Rev. Lett.* **100**, 186803 (2008).
7. R. Nandkishore, L. Levitov, *Phys. Rev. Lett.* **104**, 156803 (2010).
8. F. Zhang, H. Min, M. Polini, A. H. MacDonald, *Phys. Rev. B* **81**, 041402 (2010).
9. Y. Lemonik, I. L. Aleiner, C. Toke, V. I. Fal'ko, *Phys. Rev. B* **82**, 201408 (2010).
10. O. Vafek, K. Yang, *Phys. Rev. B* **81**, 041401 (2010).
11. V. Oganesyan, S. A. Kivelson, E. Fradkin, *Phys. Rev. B* **64**, 195109 (2001).
12. E. Fradkin, S. A. Kivelson, V. Oganesyan, *Science* **315**, 196 (2007).
13. E. Fradkin, S. A. Kivelson, M. J. Lawler, J. P. Eisenstein, A. P. Mackenzie, *Annu. Rev. Condens. Matter Phys.* **1**, 153 (2010).
14. M. P. Lilly, K. B. Cooper, J. P. Eisenstein, L. N. Pfeiffer, K. W. West, *Phys. Rev. Lett.* **82**, 394 (1999).
15. M. P. Lilly, K. B. Cooper, J. P. Eisenstein, L. N. Pfeiffer, K. W. West, *Phys. Rev. Lett.* **83**, 824 (1999).
16. R. R. Du *et al.*, *Solid State Commun.* **109**, 389 (1999).
17. Y. Ando, K. Segawa, S. Komiya, A. N. Lavrov, *Phys. Rev. Lett.* **88**, 137005 (2002).
18. V. Hinkov *et al.*, *Science* **319**, 597 (2008).
19. T. M. Chuang *et al.*, *Science* **327**, 181 (2010).
20. R. A. Borzi *et al.*, *Science* **315**, 214 (2007).
21. X. Du, I. Skachko, A. Barker, E. Y. Andrei, *Nat. Nanotechnol.* **3**, 491 (2008).
22. K. I. Bolotin *et al.*, *Solid State Commun.* **146**, 351 (2008).
23. B. E. Feldman, J. Martin, A. Yacoby, *Nat. Phys.* **5**, 889 (2009).
24. E. V. Castro *et al.*, *Phys. Rev. Lett.* **105**, 266601 (2010).
25. L. A. Ponomarenko *et al.*, *Phys. Rev. Lett.* **102**, 206603 (2009).
26. See supporting material on *Science* Online.
27. M. I. Katsnelson, *Eur. Phys. J. B* **51**, 157 (2006).
28. I. Snyman, C. W. J. Beenakker, *Phys. Rev. B* **75**, 045322 (2007).
29. J. Cserti, A. Csordás, G. Dávid, *Phys. Rev. Lett.* **99**, 066802 (2007).
30. I. M. Lifshitz, *Sov. Phys. JETP* **11**, 1130 (1960).
31. R. T. Weitz, M. T. Allen, B. E. Feldman, J. Martin, A. Yacoby, *Science* **330**, 812 (2010).
32. E. V. Castro *et al.*, *Phys. Rev. Lett.* **99**, 216802 (2007).
33. M. Mucha-Kruczyński, I. L. Aleiner, V. I. Fal'ko, *Phys. Rev. B* **84**, 041404 (2011).
34. Y.-W. Son, S.-M. Choi, Y. P. Hong, S. Woo, S.-H. Jhi, http://arxiv.org/abs/1012.0643v1 (2010).
35. R. Nandkishore, L. Levitov, *Phys. Rev. B* **82**, 115124 (2010).

Acknowledgments: This research was supported by the European Research Council, European Commision FP7, Engineering and Physical Research Council (UK), the Royal Society, U.S. Office of Naval Research, U.S. Air Force Office of Scientific Research, and the Körber Foundation.

Supporting Online Material

www.sciencemag.org/cgi/content/full/333/6044/860/DC1
SOM Text
Figs. S1 to S3

20 May 2011; accepted 29 June 2011
10.1126/science.1208683

A Synthetic Nickel Electrocatalyst with a Turnover Frequency Above 100,000 s^{-1} for H_2 Production

Monte L. Helm,[1,2]* Michael P. Stewart,[1] R. Morris Bullock,[1]† M. Rakowski DuBois,[1] Daniel L. DuBois[1]†

Reduction of acids to molecular hydrogen as a means of storing energy is catalyzed by platinum, but its low abundance and high cost are problematic. Precisely controlled delivery of protons is critical in hydrogenase enzymes in nature that catalyze hydrogen (H_2) production using earth-abundant metals (iron and nickel). Here, we report that a synthetic nickel complex, $[Ni(P^{Ph}_2N^{Ph})_2](BF_4)_2$, ($P^{Ph}_2N^{Ph}$ = 1,3,6-triphenyl-1-aza-3,6-diphosphacycloheptane), catalyzes the production of H_2 using protonated dimethylformamide as the proton source, with turnover frequencies of 33,000 per second (s^{-1}) in dry acetonitrile and 106,000 s^{-1} in the presence of 1.2 M of water, at a potential of −1.13 volt (versus the ferrocenium/ferrocene couple). The mechanistic implications of these remarkably fast catalysts point to a key role of pendant amines that function as proton relays.

Electrocatalysts that efficiently convert the energy from electricity into chemical bonds in fuels (such as hydrogen), or the reverse, converting chemical energy to electrical energy, will play a vital role in future energy storage and energy delivery systems. Hydrogenase enzymes (*1*, *2*) efficiently catalyze both the production and the oxidation of hydrogen using earth-abundant metals (nickel and iron). Detailed information about catalytic reactions of enzymes has been obtained from protein film voltammetry (*3*), but enzymes are difficult to obtain in sufficient amounts to adapt for commercial applications, and their stability is often limited outside of their native environment (*4*). Platinum is an excellent catalyst for hydrogen oxidation and production, but the scarcity and high cost of precious metals pose serious limitations to widespread use. These considerations have led to efforts to design molecular catalysts that employ earth-abundant metals. Synthetic complexes of nickel (*5*–*8*), cobalt (*9*–*12*), iron (*13*–*15*), or molybdenum (*16*, *17*) have been developed recently as electrocatalysts for the production of hydrogen.

In nature, [FeFe] hydrogenase enzymes catalyze the formation of H_2 from water, with reported rate constants as high as 9000 s^{-1} at 30°C (*18*). Crystallographic and spectroscopic studies have led to the proposal of the structure of the active site of the [FeFe] hydrogenase enzyme shown in structure **1** of Fig. 1 (*1*). The amine base positioned near the iron center has been proposed to function as a proton relay that facilitates the formation or cleavage of the H-H bond. Substantial progress on the preparation of structural mimics of the active site (*13*, *14*, *19*) provides insight into mechanistic features of the catalytic reaction. For example, Rauchfuss and co-workers have recently demonstrated that a pendant amine in a structural model closely related to **1** plays a key role in the production of H_2 (*20*). Efforts in our laboratory have focused on developing mononuclear complexes of Fe, Co, and Ni that contain an amine base in the second coordination sphere, adjacent to a vacant coordination site or a hydride ligand on the metal center (*21*–*23*). Some of these complexes are very effective electrocatalysts for H_2 formation or H_2 oxidation,

[1]Center for Molecular Electrocatalysis, Chemical and Materials Sciences Division, Pacific Northwest National Laboratory, Post Office Box 999, K2-57, Richland, WA 99352, USA. [2]Chemistry Department, Fort Lewis College, 1000 Rim Drive, Durango, CO 81301, USA.

*Sabbatical visitor at Pacific Northwest National Laboratory, 2010–2011.

†To whom correspondence should be addressed. E-mail: morris.bullock@pnnl.gov (R.M.B.); daniel.dubois@pnnl.gov (D.L.D.)